Study on the Simulation of Radial Tire Wear Characteristics

GUANG TONG AND XIAOXIONG JIN
Automotive Engineering College
Tongji University
No.4800 Caoan Road, Jiading, Shanghai
CHINA
tgmine@163.com

Abstract: - The tire wear model is build based on Archard wear theory. In this tire wear model, the steady rolling of tire is considred. Moerover, the analisys for the steady rolling of tire is used in the simulation. In this paper, 195/65R15 tire is used to build a 3D tire FE model for simulation. The tire radial direction modal and natural frequency are calculated to valitate the 3D tire FE model. At first, using Pro/E and Abaqus software the tire patten is obtained. Next, the contact footprint and pressure between tire and road are analyzed with the tire rolling dynamics. The three situations are considered to analyze the state of tire wear, the side slip angles, the vertical load and the inner pressure.

Key-Words: - Radial Tire, Steady Rolling of Tire, Tire Wear, Archard Wear Theory, Tire Radial Direction Modal, Finite element Method, ABAQUS

1 Introduction

The tire is the very important compernet of vehicles. Reducing the tire wear and improving the operating life of tire, it is necessary research for vehicle manufacturers. Moreover, tire wear is an important factor of tire noise. Tire noise is an effective noise source of vehicles. For modern passenger cars in good condition travelling at steady speed, the tyre/road interaction noise is the dominant noise source above 40 km/h. During acceleration this source is a significant contributor to the overall noise generated and above approximately 50 km/h is the dominant noise source. [1-2]. Reducing the tire wear is effective for reducing the noise of vehicles.

The process of tire wear is very complex. Tire wear can be caused by a number of factors. Some of these include incorrect inflation (outer edge wear equals low tire pressure), alignment issues, vehicle over-loading and worn out shocks or struts. In the coventional research, the tire wear is estimated by experiments [3-4]. Otherwise, the tire wear is predicted by the tire vibration and modal analysis [5-8]. Recently, with the developerment of the computer technology, the tire wear calculating with FE is a growing trend.In the early research, the tire pattern is not considered in the calculation of FE [9-15]. However, simulation results are influenced a great deal by the tire pattern.

In this paper, the tire pattern is considered in the proposed scheme. The model is based on the tire wear model using Archard wear theory. At first, using Pro/E and Abaqus software the tire patten is obtained. Next, the contact footprint and pressure between tire and road are analyzed with the tire rolling dynamics. In this paper, three situations are considered to analyze the state of tire wear, the side slip angle, the vertical load and the inner pressure.

2 Problem description and tire wear model

2.1 Radial tire contracture and tire wear

The tires of an automobile support the braking, load, traction, and steering. Tires also absorb shock caused by bumps in the road and help provide a smooth ride to the passengers. Radial car tire contracture is shown from Fig.1. Tires are made out of flexible rubber which is incorporated with wire and fabric. The typical radial tire consists of six main parts: tread, sidewall, beads, belts, carcass ply and inner liner. In this paper, the tire type is Goodyear 195/65R15. The tire width is 195mm. The tire aspect ratio is 65. The wheel diameter is 15inch. On the other hand, the outer rubber layer called the tire tread contact area directly with ground. The tread contact area is made up of a pieces of rib, lots of rubber blocks, double grooves and many slips. Tire wear is generated from the frictional slip between tread rubber blocks and ground under contact force in running motion.

Fig.2 shows the patterns of the tire uneven wear.

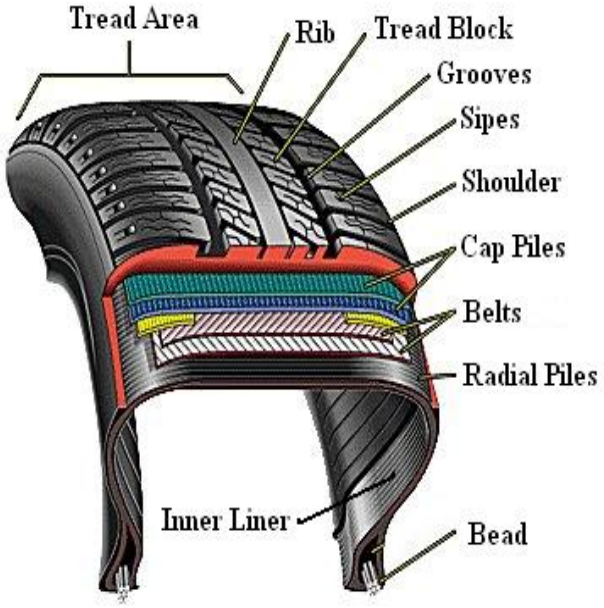

Fig.1 Radial Tire Contracture

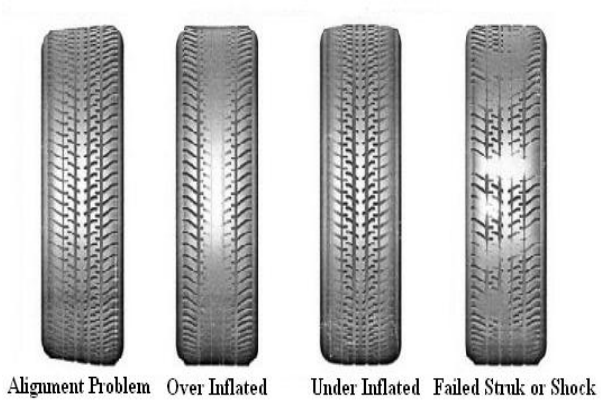

Fig.2 Tire Uneven Wear Patterns

Fig.3 Tire Uniform Wear

Differential wear at one end of the strip indicates wheel misalignment, differential wear in the center indicates over-inflation, differential wear at both ends indicates under-inflation, and differential wear around the edge on one side and a sharp edge on the other indicates failed struk or shock. In this paper, tire wear is the uniform wear, shown in Fig.3. The uniform wear is a usual normal tire wear. In Fig.3, the first tire of right side is a new tire; the first tire of left side is the approximate smooth tread; the second tire of left side is about 1/3 wear; and the third tire of left side is about 1/2 wear.

2.2 Tire wear model

To calculate the tire wear, steady rolling tire model is necessary. The slip of tire/road contact surface must be considerated. According to the situation of above, the tire wear model can be introduced.

2.2.1 Steady rolling tire model

Arbitrary Lagrangian Eulerian (ALE) formulation combines the advantages of the Lagrangian and Eulerian formulations for solving the steady-state tire rolling problem [16-19]. The general idea of ALE is the decomposition of motion into a pure rigid body motion and the superimposed deformation. This kinematic description converts the steady moving contact problem into a pure spatially dependent simulation.Using the ALE approach, the steady rolling tire model is obtained. In the following derivation, Lagrangian coordinates are denoted in uppercase and the Eulerian coordinates are denoted in lowercase. In Fig.4, A deformable body is rotating with a constant angular rolling velocity ω around a rigid axle T at X_0, which in turn rotates with a constant angular velocity Ω around the fixed X_c. The motion of a particle X at time t consists of a rigid rolling rotation to position Y, described by the following

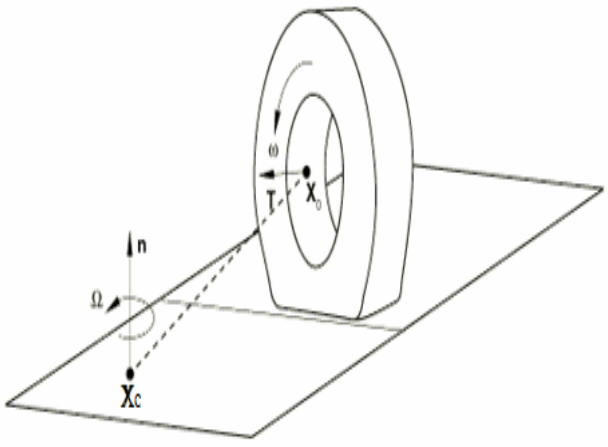

Fig.4 Steady Rolling Tire Model

equation.

$$\mathrm{Y} = \mathrm{R_s} \cdot (\mathrm{X} - \mathrm{X_0}) + \mathrm{X_0} \quad (1)$$

Where, the spinning rotation matrix $\mathrm{R_s}$ is defined as the following equation.

$$\mathrm{R_s} = \exp(\hat{\omega}_\mathrm{A} \cdot t) \quad (2)$$

Where, $\hat{\omega}_\mathrm{A}$ the skew-symmetric matrix associated with the rotation vector $\hat{\omega}_\mathrm{A} = \omega \cdot \mathrm{T}$.

This rigid rolling rotation is followed by a deformation to a point x, and a subsequent cornering rotation around n to position y so that

$$\mathrm{y} = \mathrm{R_c} \cdot (\mathrm{x} - \mathrm{X_c}) + \mathrm{X_c} \quad (3)$$

where, $\mathrm{R_c}$ is the cornering rotation given by

$$\mathrm{R_c} = \exp(\hat{\Omega}_\mathrm{A} \cdot t) \quad (4)$$

and $\hat{\Omega}_\mathrm{A}$ is the skew-symmetric matrix associated with the rotation vector $\hat{\Omega}_\mathrm{A} = \Omega \cdot \mathrm{n}$. The velocity of the particle then becomes

$$\mathrm{v} = \dot{\mathrm{y}} = \dot{\mathrm{R}}_\mathrm{c} \cdot (\mathrm{x} - \mathrm{X_c}) + \mathrm{R_c} \cdot \dot{\mathrm{x}} \quad (5)$$

To describe the deformation of the tire, a map $\chi(\mathrm{Y,t})$ is introduced, which gives the position of a point x at time t as a function of its location Y at time t so that

$$\mathrm{x} = \chi(\mathrm{Y}, \mathrm{t}) \quad (6)$$

The time derivative of (6) is given by

$$\dot{\mathrm{x}} = \frac{\partial \chi}{\partial \mathrm{Y}} \cdot \frac{\partial \mathrm{Y}}{\partial \mathrm{t}} + \frac{\partial \chi}{\partial \mathrm{t}} \quad (7)$$

where,

$$\frac{\partial \mathrm{Y}}{\partial \mathrm{t}} = \dot{\mathrm{R}}_\mathrm{s}(\mathrm{X} - \mathrm{X_0}) = \omega \mathrm{T} \times (\mathrm{Y} - \mathrm{X_0}) \quad (8)$$

Noting that $\dot{\mathrm{R}}_\mathrm{s} = \hat{\omega} \cdot R_s = \omega \hat{T} \cdot R_s$ and introducing the circumferential direction

$$\mathrm{S} = \mathrm{T} \times (\mathrm{Y} - \mathrm{X_0})/\mathrm{R} \quad (9)$$

where, $\mathrm{R} = |\mathrm{Y} - \mathrm{X_0}|$ is the radius of a point on the reference body, the velocity of the reference body can now be written as

$$\frac{\partial \mathrm{Y}}{\partial \mathrm{t}} = \omega \mathrm{RS} \quad (10)$$

and (7) can be written as

$$\dot{\mathrm{x}} = \omega R \frac{\partial Y}{\partial t} \cdot S + \frac{\partial \chi}{\partial \mathrm{t}} = \omega R \frac{\partial \chi}{\partial \mathrm{S}} + \frac{\partial \chi}{\partial \mathrm{t}} \quad (11)$$

where S is the distance-measuring coordinate along the streamline. The derivative of (4) is given by

$$\dot{\mathrm{R}}_\mathrm{c} = \hat{\Omega}_\mathrm{A} \cdot \mathrm{R_c} = \Omega \hat{\mathrm{n}} \cdot \mathrm{R_c} \quad (12)$$

The velocity of the particle can be written as the following equation.

$$\mathrm{v} = \Omega \mathrm{n} \times (\mathrm{x} - \mathrm{X_c}) + \omega R \mathrm{R_c} \cdot \frac{\partial \chi}{\partial S} + \mathrm{R_c} \cdot \frac{\partial \chi}{\partial t} \quad (13)$$

The acceleration can be obtained by differentiation of (13)

$$\begin{aligned} a = {} & \Omega^2 (\mathrm{nn\text{-}I}) \cdot (\mathrm{x\text{-}X_c}) + 2\omega\Omega R \mathrm{n} \times \mathrm{R_c} \cdot \frac{\partial \chi}{\partial S} \\ & + 2\Omega \mathrm{n} \times \mathrm{R_c} \cdot \frac{\partial \chi}{\partial t} + \omega^2 R^2 R_c \cdot \frac{\partial^2 \chi}{\partial S^2} \\ & + 2\omega R R_\mathrm{c} \cdot \frac{\partial^2 \chi}{\partial S \partial t} + R_c \cdot \frac{\partial^2 \chi}{\partial t^2} \end{aligned} \quad (14)$$

To obtain the expressions for the velocity and acceleration in the reference frame tied to the body, the following transformations are used

$$\mathrm{v_r} = R_C^T \cdot \mathrm{v},\ a_\mathrm{r} = R_C^T \cdot a \quad (15)$$

such that

$$\mathrm{v_r} = \Omega \mathrm{n} \times (\mathrm{x} - \mathrm{X_c}) + \omega R \frac{\partial \chi}{\partial S} + \frac{\partial \chi}{\partial t} \quad (16)$$

and

$$\begin{aligned} a_r = {} & \Omega^2 (\mathrm{nn\text{-}I}) \cdot (\mathrm{x\text{-}X_c}) + 2\omega\Omega R \mathrm{n} \times \frac{\partial \chi}{\partial S} \\ & + 2\Omega \mathrm{n} \times \cdot \frac{\partial \chi}{\partial t} + \omega^2 R^2 \frac{\partial^2 \chi}{\partial S^2} \\ & + 2\omega R \frac{\partial^2 \chi}{\partial S \partial t} + \frac{\partial^2 \chi}{\partial t^2} \end{aligned} \quad (17)$$

For steady-state conditions it holds that $\frac{\partial \chi}{\partial t} = 0$ and these expressions can be reduced to the following equations.

$$\mathrm{v_r} = \Omega \mathrm{n} \times (\mathrm{x} - \mathrm{X_c}) + \omega R \frac{\partial \chi}{\partial S} \quad (18)$$

$$\begin{aligned} a_r = {} & \Omega^2 (\mathrm{nn\text{-}I}) \cdot (\mathrm{x\text{-}X_c}) + 2\omega\Omega R \mathrm{n} \times \frac{\partial \chi}{\partial S} \\ & + \omega^2 R^2 \frac{\partial^2 \chi}{\partial S^2} \end{aligned} \quad (19)$$

The first term of (19) can be seen as the acceleration that gives rise to centrifugal forces resulting from rotation about n. The second term can be identified as the acceleration that gives rise to Coriolis forces. The last term combines the acceleration that give rise to Coriolis and centrifugal forces resulting from rotation about T. When the deformation is uniform along the circumferential direction, both Coriolis effects vanishes so that the acceleration gives rise to centrifugal forces only.

The velocity of the center of the body $\mathrm{X_0}$ is given by the following equation.

$$\mathrm{v_0} = \Omega \mathrm{n} \times (\mathrm{x} - \mathrm{X_c}) \quad (20)$$

Since the motions due to rolling and deformation vanish on the axis. In the case of straight line rolling $\Omega = 0$, (18) and (19) can be reduced to the following equations.

$$\mathrm{v} = \mathrm{v}_0 + \mathrm{v}_\mathrm{r} = \mathrm{v}_0 + \omega R \frac{\partial \chi}{\partial S} \tag{21}$$

$$a = a_r = \omega^2 R^2 \frac{\partial^2 \chi}{\partial S^2} \tag{22}$$

2.2.2 The slip of tire/road contact surface

Given two points on the surfaces of two bodies in contact, the relative velocity can be expressed as the following equation.

$$\mathrm{v} = \mathrm{v}_\mathrm{D} - \mathrm{v}_\mathrm{R} \tag{23}$$

Where, v_D is the velocity of a point on the deformable body, see (16), and v_R the velocity of a point on the rigid foundation. This can be split into the normal and tangential components. The rate of penetration is the following equation.

$$\dot{\mathrm{h}} = -\mathrm{n} \cdot \mathrm{v} = \mathrm{n} \cdot \mathrm{v}_\mathrm{R} - \omega R \mathrm{n} \cdot \frac{\partial \chi}{\partial S} - \mathrm{n} \cdot \frac{\partial \chi}{\partial t} \tag{24}$$

For any point in contact it follows that $\mathrm{n} \cdot \frac{\partial \chi}{\partial S} = 0$,

therefore

$$\dot{\mathrm{h}} = -\mathrm{n} \cdot \mathrm{v}_\mathrm{R} - \mathrm{n} \cdot \frac{\partial \chi}{\partial t} \tag{25}$$

The rate of slip is given by the following equation.

$$\dot{\gamma}_\alpha = \mathrm{t}_\alpha \cdot \mathrm{v} = \Omega \mathrm{t}_\alpha (\mathrm{n} \times \mathrm{r}) + \omega R \mathrm{t}_\alpha \frac{\partial \chi}{\partial S} + \mathrm{t}_\alpha \frac{\partial \chi}{\partial t} - \mathrm{t}_\alpha \cdot \mathrm{v}_\mathrm{R} \tag{26}$$

where, $\mathrm{t}_\alpha (\alpha = 1,2)$ are two orthogonal unit vectors tangent to the contact surface such that $\mathrm{n} = \mathrm{t}_1 \times \mathrm{t}_2$.

For steady-state conditions it holds that $\frac{\partial \chi}{\partial t} = 0$,

which gives the final expression for the slip velocity

$$\dot{\gamma}_\alpha = \mathrm{t}_\alpha \cdot \mathrm{v} = \Omega \mathrm{t}_\alpha (\mathrm{n} \times \mathrm{r}) + \omega R \mathrm{t}_\alpha \frac{\partial \chi}{\partial S} - \mathrm{t}_\alpha \cdot \mathrm{v}_\mathrm{R} \tag{27}$$

In the line rolling conditions, $\Omega \mathrm{n} \times \mathrm{r}$ can be replaced by v_0 , then the slip velocity can be described as follows.

$$\dot{\gamma}_\alpha = \mathrm{t}_\alpha \cdot \mathrm{v}_0 + \omega R \mathrm{t}_\alpha \cdot \frac{\partial \chi}{\partial S} - \mathrm{t}_\alpha \cdot \mathrm{v}_\mathrm{R} \tag{28}$$

2.2.3 Tire wear model

The Archard wear theory is a simple model used to describe sliding wear and is based around the theory of asperity contact. The calculation of adhesive wear is proposed by Archard. In this paper, the tire wear model is based on Archard wear theory [20-24]. The equation of Archard wear theory is described as follows.

$$V = K \frac{F_N}{H} L \tag{29}$$

Where, V is the total volume of wear amount, K is the wear coefficient, $\mathrm{F_N}$ is the normal load of contact pair, H is the hardness of the soft mertial in the contact pair, L is the slip distance.

From the realition $F_N = PA$, the following equation is obtained.

$$V = K \frac{PA}{H} L \tag{30}$$

Where, P is the normal pressure of contact surface, A is the contact area.

In the process of tire rolling, the slip distance is shown by the following equation.

$$L = \dot{\gamma} \cdot t \tag{31}$$

Where, $\dot{\gamma}$ is the slip ratio, t is the virable of time. Then, the ratio of volume wear is described as follows.

$$\dot{V} = K \frac{PA}{H} \dot{\gamma} \tag{32}$$

The tire surface can be considered as a lot of ribbions, the center line of every ribbion consists of many nodes as a dash line. Assuming the wear of every ribbion is average in the circlular direction, the ratio of volume wear for every ribbion is generated by the following equation.

$$\dot{V} = \frac{K}{H} \int_{ribbon} P(x,t) \dot{\gamma}(x,t) dA \tag{33}$$

Where, x is the variable of position.

The stead state motion is calculated by Euler's steady state transport, the ratio of volume wear for every ribbion is can be described as follows.

$$\dot{V} = \frac{K}{H} \int_s P(s) \dot{\gamma}(s) T(s) ds \tag{34}$$

Where, s is the positional variable along the direction of steamline, $T(s)$ is the width of ribbion at the position s .

From Discrete form, the following equation is obtained.

$$\sum_{i=1}^{N} \dot{h}_i A_i = \frac{K}{H} \sum_{i=1}^{N} P_i \dot{\gamma}_i T_i \tag{35}$$

Where, N is the number of nodes for the center dash line, $\dot{h}_i$ is the ratio of wear for node i the center dash line, A_i is the cotact area near node i , T_i is the

Table 1 Material Property of Tire Components

Tire components	Radial ply	Sidewall	Shoulder	Inner liner	Belt
Material	Nylon	Rubber	Rubber	Rubber	Steel
Density(kg/m^3)	9000	1100	1100	1100	5900
C10	0.671	0.336	1.006	0.671	0.83
D1	0.03	0.01	0.02	0.03	0.024

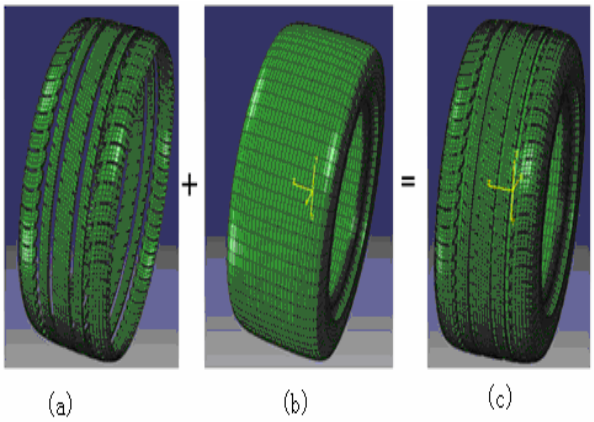

Fig.4 Tire FE model

Fig.5 Tire Modal Test

width of ribbon near node i .

Because of assuming the wear of every ribbion is average in the circlular direction, the ratio of wear is described as follows.

$$\dot{h} = \frac{\frac{K}{H}\sum_{i=1}^{N} P_i \dot{\gamma}_i T_i}{\sum_{i=1}^{N} A_i} \tag{36}$$

3 Tire FE Model

3.1 Tire material property

Rubber is by nature a near-incompressible and hyperelastic material with viscoelasticity. However, the tire industry does not usually make public the exact material properties used in tire design. In this study, the rubber is simulated as a linear elastic material with Poisson's ratio close to 0.5. Different parts of rubber elements (sidewall, shoulder, belt rubber, and tread) are modeled using variable elastic stiffness. The steel reinforcements (radial ply and belts) are modeled as a linear elastic material with high modulus [25]. In the tire model, the rubber components are modeled by the Neo-Hooken hyperelastic and the reinforcing fibres are represented by the linear elastic material models, respectively. The Neo-Hooken equation is shown as follows.

$$U = C_{10}(\bar{I}_1 - 3) + \frac{1}{D_1}(J-1)^2 \tag{37}$$

Where, the values of C_{10}, D_1 are shown in Table. 1.

The tire tread model is built by the linear elastic material model. In this model, Young's modulus is 6MPa; Poisson's ratio is 0.49.

3.2 Tire FE model

To build the tire wear model, at first, using Pro/E, 3D tire surface pattern model is build. Next, using Abaqus FE software, meshes for the tire surface pattern model is set with the 3D tire surface pattern model, shown in Fig.4 (a). The tire body model is based on construct and geometric symmetry of material properties. Using the functions of Abaqus FE software, the axial symmetry model of tire body can be obtained. From the rotation of the axial symmetry model, the 3D tire body FE model is generated, shown in Fig.4 (b). At last, tying tire surface pattern model and tire body model together, the final tire FE model [26] can be obtained, shown in Fig.4 (c). The final tire FEM model has 80943 nodes and 66663 elements.

3.3 Model Verification

In this paper, the effectiveness of tire FE model is verified by extracting the tire radial directional natural frequency. The comparison between the results of modal test and simulation is applied.

The equipment of modal test is shown in Fig.5. During the test, inner air pressure is maintained at 0.25MPa. 84 measuring points (12 points of them in circumferential direction and 7 circles in tread-width

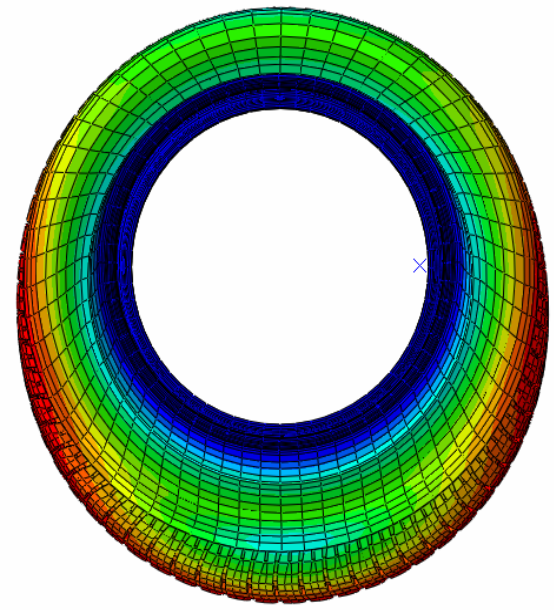

(a) first–order modal

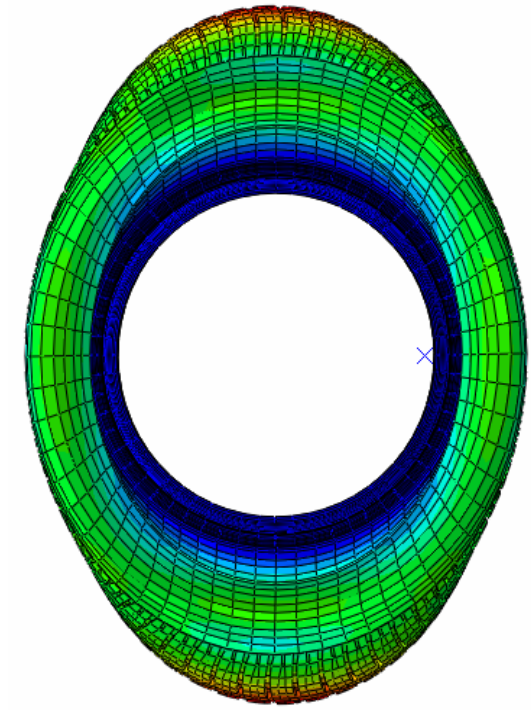

(b) second–order modal

Fig.7 Tire Modal Shape (1)

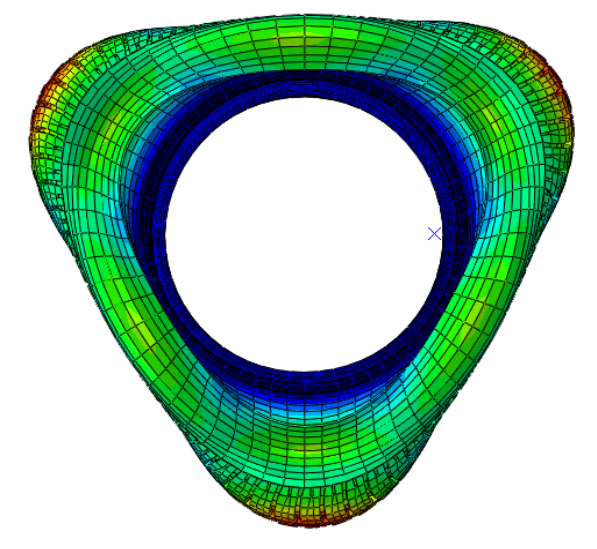

(a) third–order modal

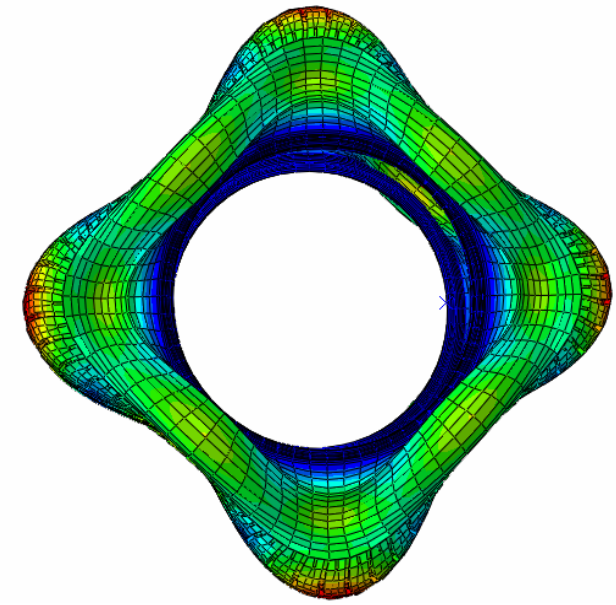

(b) fourth–order modal

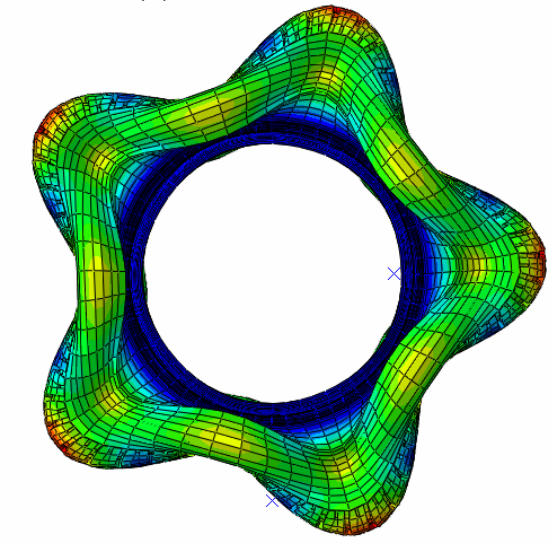

(c) fifth–order modal

Fig.7 Tire Modal Shape (2)

Table 2 Test and Simulation Comparison

Order	Test Frequency/Hz	Simulation Frequency/Hz	Deviation/%
1	64.8	63.9	-1.39
2	90.2	90.3	0.11
3	113.3	115.8	2.21
4	149.5	141.8	-4.48
5	171.2	167.5	-2.16

direction) are set up on the tire to obtain its vibration characteristics fully and clearly. Every point is measured three times in *x*, *y* and *z* direction respectively.

The test frequency is from 0 Hz to 500 Hz and the tire is excited by a random signal.

The tire radial directional modals are shown in Fig.6 and Fig.7. Fig.6 (a) is the simulation results of the first–order modal; Fig.6 (b) is the simulation results of the second–order modal. Fig.7 (a) is the simulation results of the third–order modal; Fig.7 (b) is the simulation results of the fouth–order modal; Fig.7 (c) is the simulation results of the fifth–order modal.The comparison between the results of modal test and simulation is summarized in Table 2. Each modal frequency in simulation shows good agreement with the test results and the maximum deviation is 4.48%.

From the tire modal analysis, we can surely conclude that the reliability and accuracy about the vibration characteristics of the tire FE model are verified.

4 Simulation Results

4.1 Tire static contact pressure

For the tire model considering the complx pattern, in case of low vertical load, the contact footprint is close to ellipse; in case of high vertical load, the contact footprint is close to rectangle. Because the center of tire contact is extruded as the concave, the pressure at the tire footprint center is smaller than the pressure of peripheral areas. However, beacause the discontinuity of rubber block occurs from the lateral and longitudinal groove, the cantact pressure distributes regularly according to the tire pattern, shown in Fig.8. Fig.8 (a) is the simulation result of contact pressure with static load 300N; Fig.8 (b) is contact pressure with static load 600N; Fig.8 (c) is contact pressure with static load 1800N; and

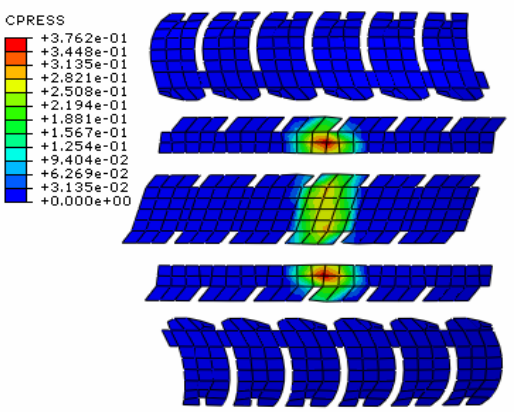

(a) Static Load 300N

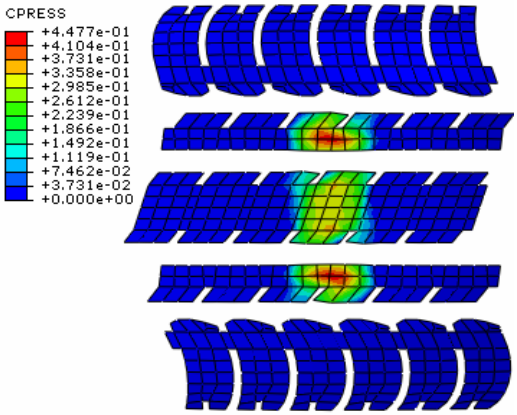

(b) Static Load 600N

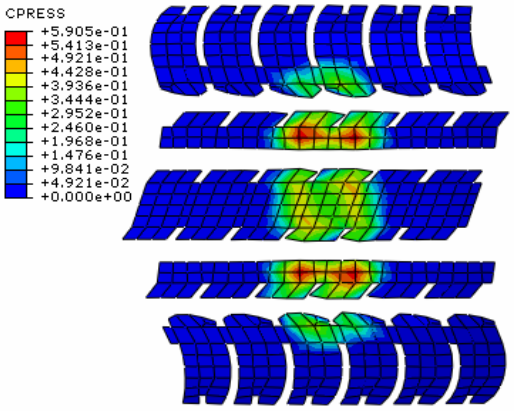

(c) Static Load 1800N

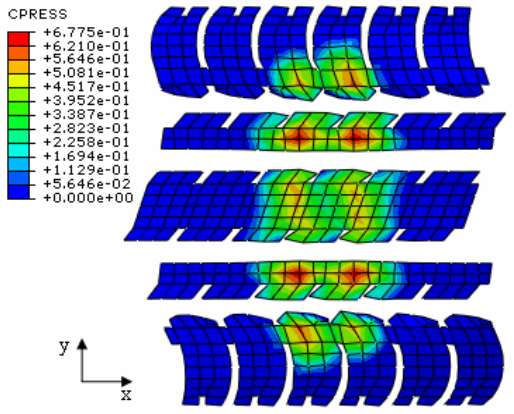

(d) Static Load 3000N

Fig.8 Contact pressure with static load (MP_a)

Fig.8 (d) is contact pressure with static load 3000N.

From Fig.8, it can be seen that the contact pressure distributes regularly. Increasing the static load, the contact area increases, the contact pressure is diffused from the center to peripheral areas. All contact footprints can keep the ellipse form, however, all contact footprints are divided into the different parts, the distribution of contact pressure is discontinuous in all contact footprints. From lateral direction, the pressure at two pattern of tire shoulder is high. From longitudinal direction, the pressure distribution relates to the form of pattern.

4.2 The influence of slip angle for tire wear

The slip angle is the angle between a rolling wheel's actual direction of travel and the direction towards which it is pointing. In case of different slip angles, the pressure distribution of the cantact footprint is shown in Fig.9. Fig.9 (a) is the simulation result of contact pressure with slip angle 0°; Fig.9 (b) is contact pressure with slip angle 1°; Fig.9 (c) is contact pressure with slip angle 2°; and Fig.9 (d) is contact pressure with slip angle 3°.

From Fig.9 (a), it can be seen that the cantact footprints are symmetric distribution. From Fig.9 (b), (c) and (d), it is clear that increasing the slip angle, the contact pressure moves in the tire slip direction, the contact footprints have the same variation. At the same time, because the slip angle exists, the distortion occurs at the peripheral areas of the contact footprint pattern. This distortion influence the tire wear greatly, therefore, the partial wear is generated on the surface of tire.

The wear depth of tire surface with different slip angles is shown in Fig.10. The wear depth means the wear amount of tire pattern groove in the lateral direction of the tire surface. From Figure 4, it can be seen that the partial wear is generated on the surface of tire by the existence of slip angles so that the wear depth in the direction of slip is larger than the wear depth of another side. At the same time, because the slip angle exists, the tire surface pattern influences the tire wear deeply, it is clear that the wear depth for the pattern block of tire shoulder has greatly variations. Increasing the slip angle, the wear depth in the direction of slip increases, meanwile, and the wear depth at another side reduces. However, the increasing amount of tire wear in the direction slip is higher than the reducing amount of tire wear at another side. From the fact of

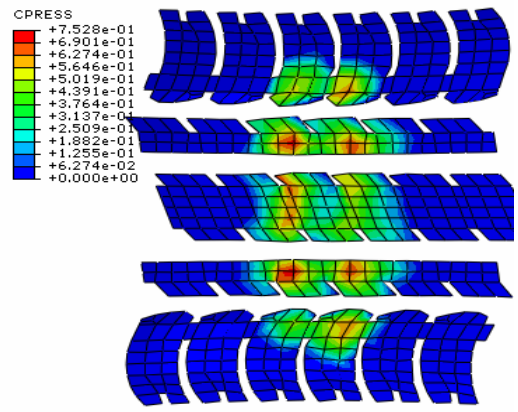

(a) Slip Angle 0°

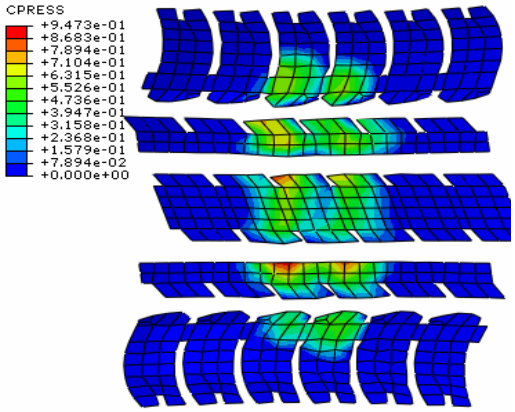

(b) Slip Angle 1°

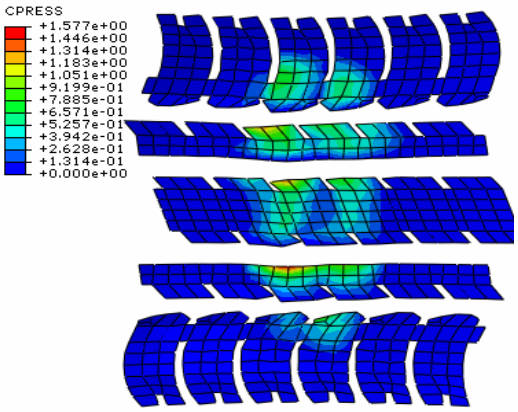

(c) Slip Angle 2°

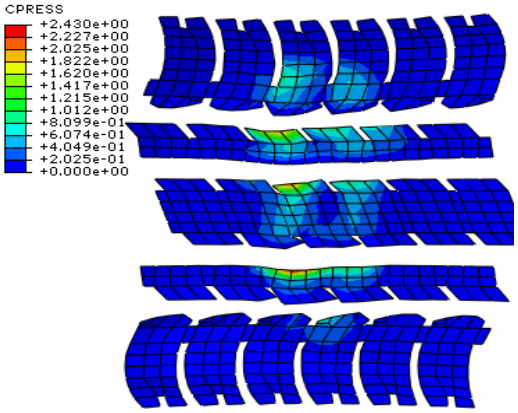

(d) Slip Angle 3°

Fig.9 Contact pressure with slip angle (MP_a)

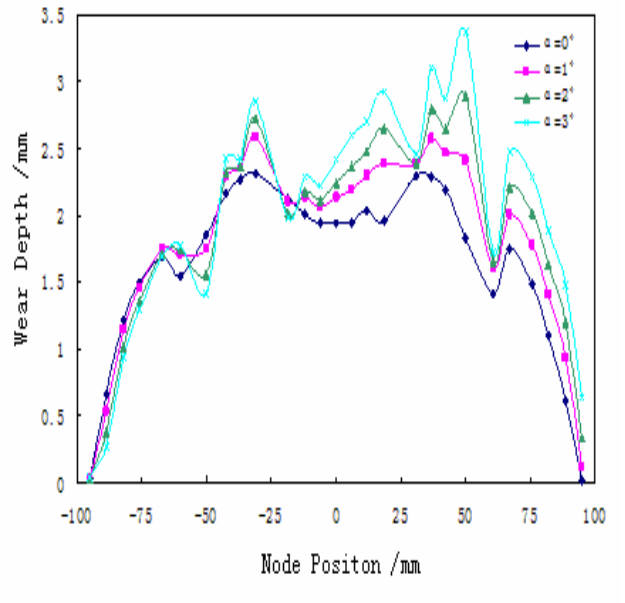

Fig.10 The wear depth of tire pattern with slip angle

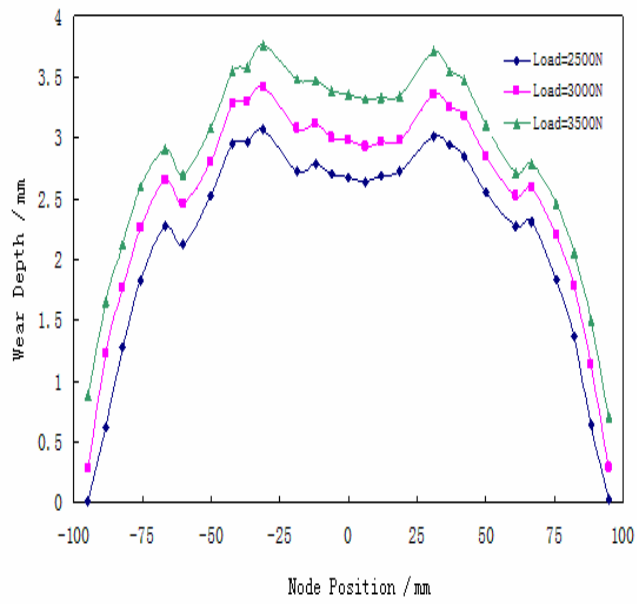

Fig.11 The wear depth of tire pattern with vertical load

above, it can be seen that the tire wear is not uniform, and the total tire wear also increase.

4.3 The influence of vertical load for tire wear

The simulation conditions are set as: tire rolling velocity is 32*km/h*, tire rolling angle velocity is 34.6*rad/s*, tire rolling distance is 32000*km*. The vertical loads are set as: 2500*N*，3000*N* and 3500*N*. The wear state of tire surface is calculated with these three different vertical loads, and the influence of vertical load for tire wear is analyzed.

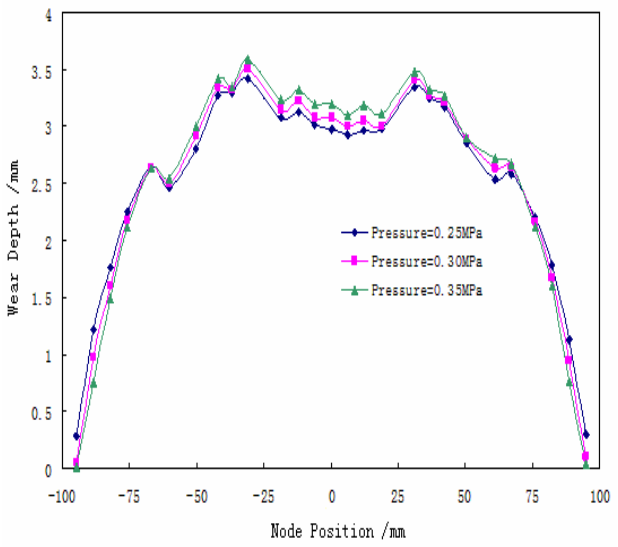

Fig.12 The wear depth of tire pattern with inner pressure

In Fig.11, the simulation result for the lateral wear depth of tire surface is shown. From Fig.11, it can be seen that increaing the vertical load, the wear depth of tire surface increases, and then, the relation between the increasing wear amount of every part and the increasing amount of vertical load is closed to linear. For different pattern blocks, the increaing amount of wear depth in the center part of tire surface is smaller than the increaing amount of wear depth at both sides.

4.4 The influence of inner pressure for tire wear

The simulation conditions are set as: tire rolling velocity is 32*km/h*, tire rolling angle velocity is 34.6*rad/s*, tire rolling distance is 32000*km*. The inner pressures of tireare set as: 0.25 MPa，0.30 MPa and 0.35 MPa. The wear state of tire surface is calculated with these three different inner pressures, and the influence of inner pressure for tire wear is analyzed.

Fig.12 shows the lateral wear depth of tire surface. From Fig.12, it can be seen that the inner pressure influences the wear of tire surface. At first, increaing the inner pressure, the wear depth in the center part of tire surface increases, and then, the wear depth at the both sides reduces. Next, compared with the situation of the vertical load, the same increasing amount of inner pressure influences tire wear smaller.

5 Conclusion

In this paper, based on the tire wear model using

Archard wear theory, a 3D tire FE model is built. At first, using Pro/E and Abaqus software the tire patten is obtained. Next, the contact footprint and pressure between tire and road are analyzed with the tire rolling dynamics. The tire pattern is considered. Three situations are considered to analyze the state of tire wear, the side slip angle, the vertical load and the inner pressure. From simulation and analysis, it can be conclued as follows.

(1) All contact footprints can keep the ellipse form, however, all contact footprints are divided into the different parts, the distribution of contact pressure is discontinuous in all contact footprints. From lateral direction, the pressure at two pattern of tire shoulder is high. From longitudinal direction, the pressure distribution relates to the form of pattern.

(2) The partial wear is generated on the surface of tire by the existence of slip angles so that the wear depth in the direction of slip is larger than the wear depth of another side.

(3) Increaing the vertical load, the wear depth of tire surface increases, and then, the relation between the increasing wear amount of every part and the increasing amount of vertical load is closed to linear. For different pattern blocks, the increaing amount of wear depth in the center part of tire surface is smaller than the increaing amount of wear depth at both sides.

(4) Increaing the inner pressure, the wear depth in the center part of tire surface increases, and then, the wear depth at the both sides reduces. Compared with the situation of the vertical load, the same increasing amount of inner pressure influences tire wear smaller.

References:

[1] Reaz Ahmed S., Deb Nath S. K., Wahhaj Uddin M., Optimum Shapes of Tire-treads for Avoiding Lateral Slippage between Tires and Roads, International Journal for Numerical Methods in Engineering, No.64, 2005, pp. 729-750.

[2] O'Boy D.J., Dowling A.P., Tyre/road Interaction Noise-Numerical Noise Prediction of a Patterned Tyre on a Rough Road Surface, Journal of Sound and Vibration, No.323, 2009, pp. 270-291.

[3] Walters, M. H., Uneven Wear of Vehicle Tires, Journal of Tire Science and Technology, Vol.21, No.4, 1993, pp. 202-219.

[4] Manas D., Manas M., Pat V., Wear of Tyre Treads. Journal of Achievements in Materials and Manufacturing Engineering, Vol.37, No.2, 2009, pp. 538-543.

[5] Burke, A.M., Olatunbosun, O.A., Contact Modelling of the Tyre/road Interface, International Journal of Vehicle Design, Vol.18, No.2, 1997, pp. 194-202.

[6] Cho J.R., Shin S.W., Yoo W.S., Crown shape optimization for enhancing tire wear performance by ANN, Computers and Structures, No.68, 2005, pp. 920-933.

[7] Braghin F., Cheli F., Melzi S., Resta F., Tyre Wear Model: Validation and Sensitivity Analysis, Meccanica, No.41, 2006, pp. 143-156.

[8] Kim B. S., Chi C. H., Lee T. K., A Study on Radial Directional Natural Frequency and Damping Ratio in a Vehicle Tire, Applied Acoustics, No.68, 2007, pp. 538-556.

[9] Danielson K. T., Noor A. K., Green J. S., Computational Strategies for Tire Modeling and Analysis, Computers & Structures, Vol.61, No.4, 1996, pp. 673-693.

[10] Becker, A., Seifert, B., Simulation of Wear with A FE Type Model Using A Steady State Rolling Formulation, International Conference on Contact Mechanics, Proceedings, 1997, pp. 119-128.

[11] Zhang, X., Rakheja, S., Ganesan, R., Estimation of Tyre-road Contact Pressure Distribution Based on Nonlinear Finite Element Analysis, Journal of Heavy Vehicle Systems, Vol.8, No.3, 2001, pp. 197-217.

[12] Dorsch, V., Becker, A., Vossen, L., Enhanced Rubber Friction Model for Finite Element Simulations of Rolling Tyres, Journal of Plastics, Rubber and Composites, Vol.31, No.10, 2002, pp. 458-464.

[13] Ghoreishy, M.H.R., Finite Element Analysis of Steady Rolling Tyre with Slip Angle: Effect of Belt Angle, Journal of Plastics, Rubber and Composites, Vol.35, No.2, 2006, pp. 83-90.

[14] Ghoreishy, Mir Hamid Reza., A State of the Art Review of the Finite Element Modelling of Rolling Tyres, Journal of Iranian Polymer, Vol.17, No.8, 2008, pp. 571-597.

[15] Ghoreishy, Mir Hamid Reza., Finite Element Modelling of the Steady Rolling of a Radial Tyre with Detailed Tread Pattern, Journal of Iranian Polymer, Vol.18, No.8, 2009, pp. 641-650.

[16] Nackenhorst U., The ALE-Formulation of Bodies in Rolling Contact Theoretical Foundations and Finite Element Approach, Computer Methods in Applied Mechanics and Engineering, No.193, 2004, pp. 4299–4322.

[17] Ziefle, M., Nackenhorst U., A New Update Procedure for Internal Variables in an ALE Description of Rolling Contact, Proceedings in

Applied Mathematics and Mechanics, No.5, 2005, pp. 71–74.
[18] Laursen, T.A, Stanciulescu, I., An Algorithm for Incorporation of Frictional Sliding Conditions within a Steady State Rolling Framework. Communications in numerical methods in engineering, No.22, 2006, pp. 301–318.
[19] Neri F., Learning and Predicting Financial Time Series by Combining Natural Computation and Agent Simulation, Applications of Evolutionary Computation, Lecture Notes in Computer Science 6625, 2011, pp. 111-119.
[20] Archard J. F., Contact and Rubbing of Flat Surfaces, Journal of Applied Physics, Vol.24, No.8, 1953, pp. 981-988.
[21] Zglimbea R., Finca V., Greaban E., Constantin M., Research on Parameter Identification of Modified Friction LuGre Model Based Distributions Theory, *WSEAS TRANSACTIONS on SYSTEMS*, Vol.8, No.8, 2009, pp. 978-987.
[22] Li Y., Zhang J. W., Guan X. Q., Estimation of Vehicle Parameters and Road Friction Using Steering Torque and Wheel Speeds, *WSEAS TRANSACTIONS on SYSTEMS*, Vol.11, No.1, 2012, pp. 1-11.
[23] ZHANG Y. CH., ZHANG G.G., YU F., Modeling and μ Synthesis Control of Vehicle Active Suspension with Motor Actuator, *WSEAS TRANSACTIONS on SYSTEMS*, Vol.11, No.5, 2012, pp. 173-186.
[24] Tong G., Wang Q., Jin X. X., Adaptive Lane Keeping Control of Vehicles with Tire Influence, International journal of Advancements in Computing Technology, Vol.4, No.18, 2012, pp. 433-439.
[25] Yin W., Jin X. X., Tong G., Finite Element Analysis of Rubber Constitutive Models and Simulation, Journal of Shanghai Dianji University, Vol.13, No.4, 2010, pp. 215-218.
[26] Tong G., Jin X. X., Hou Ch. Y., Modeling Car Tread Patterns Using Pro/Engineer, Journal of Shanghai Dianji University, Vol.14, No.1, 2011, pp. 35-38.